Nanoscale Advances

ROYAL SOCIETY OF CHEMISTRY

PAPER

View Article Online
View Journal | View Issue

Check for updates

Cite this: *Nanoscale Adv.*, 2022, **4**, 3282

Monolayer $NaW_2O_2Br_6$: a gate tunable near-infrared hyperbolic plasmonic surface†

Enhui Huang,‡[a] Hui Xiang, ‡[b] Han Jiao,[a] Xia Zhou,[a] Jinli Du,[a] Wenying Zhong *[a] and Bo Xu *[a]

Received 9th May 2022
Accepted 4th July 2022

DOI: 10.1039/d2na00292b

rsc.li/nanoscale-advances

Electrically tunable hyperbolic polaritons in two dimensional (2D) materials can offer unexplored opportunities in integrating photonics and nano-optoelectronics into a single chip. Here, we suggest that monolayer $NaW_2O_2Br_6$ can host electrically tunable hyperbolic plasmon polaritons for infrared light *via* first-principles calculations. 2D monolayer $NaW_2O_2Br_6$ exhibits an extremely anisotropic metallic property: conducting for one direction but almost insulating for the other direction, which could be considered as a 2D analogue of metal/dielectric multilayers, a typical structure for hyperbolic metamaterials. More interestingly, we also demonstrate that the hyperbolic properties in the near-infrared range, including the hyperbolic windows, figure of merit, and propagation directions of plasmon beams, can be effectively modulated by carrier doping at the order of 10^{13} cm^{-2}, which even can be accessed by solid-gated field effect transistors. Thus, it is anticipated that monolayer $NaW_2O_2Br_6$ has a great potential in constructing field programmable polariton nanodevices for emerging and diverse photonic applications.

Introduction

Because of the extraordinary ability to control light down to the atomic length-scale, two dimensional (2D) materials hosting hyperbolic polaritons have emerged as one of the most attractive research interests in the past few years.[1–3] In particular, several 2D materials, such as BN,[4–6] MoO_3,[7–10] and V_2O_5,[11] have been demonstrated to possess hyperbolic phonon polaritons (PhPs) with excellent properties, such as long lifetimes, low loss and strong field confinement, and offer as yet unexplored opportunities for photonic and optoelectronic devices. However, hyperbolic PhPs, the hybrid excitation of light and lattice vibration, usually are hard to control and tune by electric fields, indicating that it still remains a challenge to integrate hyperbolic PhPs into nanophotonic and optoelectronic circuits.

Compared to PhPs, plasmon polaritons (PPs)[12,13] show great potential in gate control devices, because of the dependence of plasma frequency (ω_p) on the carrier density: $\omega_p{}^2 = ne^2/\varepsilon_0 m^*$, in which n is the carrier density, and m^* is the effective mass of the carrier. Graphene,[14] a special 2D metal with no intrinsic carrier, is a perfect carrier tunable plasmonic material. Periodic graphene strips[15,16] are suggested to exhibit tunable hyperbolic PPs in the THz region due to the adjustable Fermi levels upon the gate voltages. WTe_2, an anisotropic semimetal, was demonstrated to be a natural hyperbolic plasmonic surface in the far-IR range.[17,18] 2D in-plane anisotropic semiconductors, such as black phosphorus[19,20] and TiS_3,[21] are theoretically proposed to exhibit natural tunable hyperbolic plasmonic behaviors for near infrared (NIR) light by carrier doping. However, these proposed hyperbolic PPs in the NIR range can be realized only when the carrier densities reach 10^{14} cm^{-2}. Recently, anisotropic 2D metals, such as boron,[22,23] $MoOCl_2$,[24] and CuB_3,[25] are indicated as natural hyperbolic surfaces due to their anisotropic metallic properties. Attributed to their high intrinsic carrier densities, up to 10^{15} cm^{-2}, outstanding hyperbolic PPs, such as low losses and wide hyperbolic windows, can even work in the visible light range. But just because of the high intrinsic carrier concentrations, these hyperbolic PPs in 2D metals usually are not sensitive to the gate voltages. To modulate these plasmonic properties by carriers, the tunable carrier density should be up to 10^{14} cm^{-2} at least. As we see, despite the potential of these hyperbolic PPs for on-chip photonic devices, candidates with electrically tunable hyperbolic PPs are still rare, especially in the short wave range, attributed to the high required carrier density, up to 10^{14} cm^{-2}. Thus, from an integration perspective, it is urgent to explore electrically tunable hyperbolic PPs.

Herein, based on first-principles calculations, we found that monolayer $NaW_2O_2Br_6$ is a potential candidate for electrically tunable hyperbolic PPs for NIR light. Monolayer $NaW_2O_2Br_6$

[a]*School of Science and Key Laboratory of Biomedical Functional Materials, China Pharmaceutical University, Nanjing 211198, P. R. China. E-mail: wyzhong@cpu.edu.cn; xubo@cpu.edu.cn*

[b]*School of Mathematics and Physics, Hubei Polytechnic University, Huangshi, 435003, P. R. China*

† Electronic supplementary information (ESI) available. See https://doi.org/10.1039/d2na00292b

‡ These authors contributed equally: Enhui Huang, and Hui Xiang.

could be regarded as a 2D analogue of metal/dielectric multilayers owing to its extremely anisotropic metallic property, conducting for one direction but almost insulating for the other direction. It results in monolayer $NaW_2O_2Br_6$ with natural hyperbolic PPs for infrared light. Due to low intrinsic carrier concentration, only about 2.5×10^{14} cm^{-2}, the hyperbolic PPs in the NIR range are suggested to be tunable even by solid-gated field effect transistors (FETs), which shows great advantages in integrated optical devices.

Results

Anisotropic crystal structure of monolayer $NaW_2O_2Br_6$

Orthorhombic $NaW_2O_2Br_6$ was experimentally reported as a layered material with mixed valence tungsten.[26] The optimized crystal structure of monolayer $NaW_2O_2Br_6$ is displayed in Fig. 1a with a large unit cell size of about 40 $Å^2$ (a = 3.82 Å, and b = 10.54 Å). Detailed structure information is supplied in the ESI (Table S1†). As we see, monolayer $NaW_2O_2Br_6$ exhibits an extremely anisotropic crystal structure. The W atoms are sixfold coordinated by two O atoms and four Br atoms to form $[WO_2Br_4]$ octahedra, which are condensed to pairs *via* a common Br_2 edge and condensed *via* the oxygen ligands to form 1D $[W_2O_2Br_6]^-$ anionic chains along the x direction. These 1D chains are interconnected by the Na^+ cations to form a 2D structure. By counting the electron number, we found that there is one electron per unit cell, resulting in a carrier concentration of 2.5×10^{14} cm^{-2}, about one order less than those in traditional 2D metals, such as boron[22,23] and TaS_2.[27] By the carrier density mapping in Fig. 1b, we see that a one-dimensional electron gas (1DEG) is confined primarily in the $[W_2O_2Br_6]$ chains and separated by Na^+ cations. As can be seen from the line plot in Fig. 1c, the width of the 1DEG is about 0.5–0.6 nm. The inhomogeneous carrier distribution in monolayer $NaW_2O_2Br_6$ indicates an extremely anisotropic metallic behavior: conducting along the x direction, but almost insulating along the y direction. It looks like a natural 2D metal/dielectric multilayer (Fig. 1d), which is a typical structure to design hyperbolic metamaterials.[28] Thus, monolayer $NaW_2O_2Br_6$ may be a natural candidate to host hyperbolic PPs. Moreover, the periodicity of a metal/dielectric multilayer in monolayer $NaW_2O_2Br_6$ is only about 1 nm, about one order less than those in traditional metal/dielectric multilayered hyperbolic metamaterials.[28] Such hyperbolic PPs in natural materials have significant advantages for potential applications. Apparently, they not only can avoid complex fabrication processes for hyperbolic devices. Compared to metamaterials, natural materials have much larger Brillouin zones, which can overcome the limitation of wave vectors attributed to the size of the Brillouin zone.[10,28]

Anisotropic electronic and optical properties of monolayer $NaW_2O_2Br_6$

Before investigating the hyperbolic properties in monolayer $NaW_2O_2Br_6$, we first performed density functional theory (DFT) calculations (see Methods) for its electronic properties. Fig. 2a displays the calculated orbital projected band structure for monolayer $NaW_2O_2Br_6$, obtained from HSE hybrid density functional calculations. d_{xz} and d_{xy} orbitals of W dominate the low energy states around the Fermi level, with little hybridization with Br-4p orbitals. Based on the band structure, monolayer $NaW_2O_2Br_6$ is an extremely anisotropic metal. Usually, the anisotropy of a metal is expressed by different dispersions for

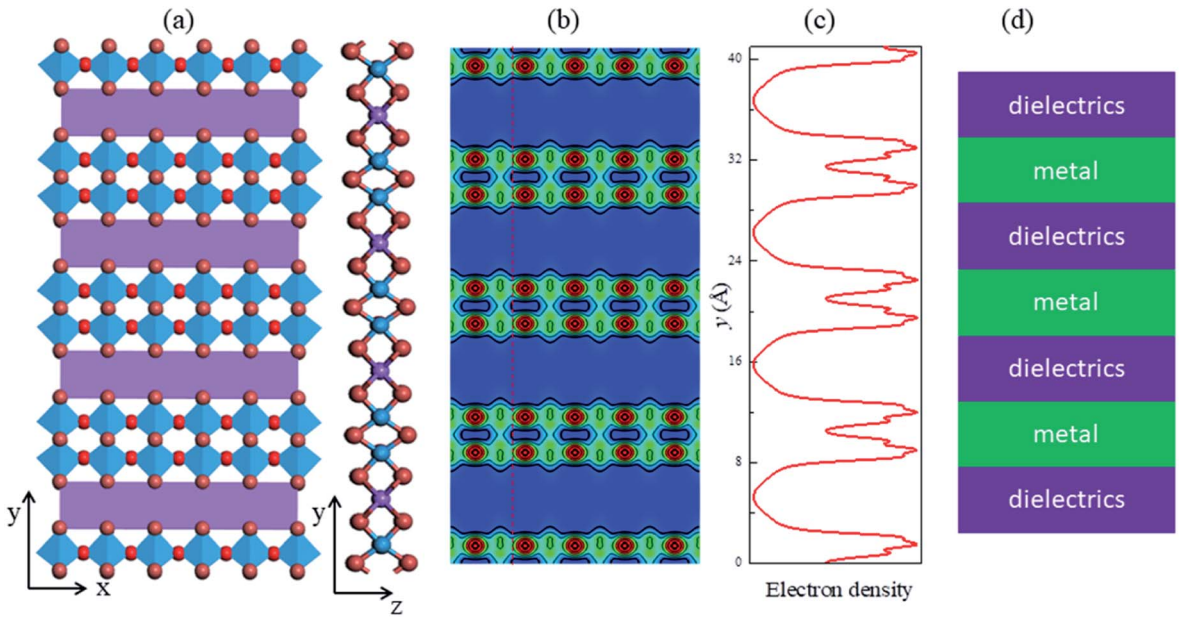

Fig. 1 Anisotropic structure of monolayer $NaW_2O_2Br_6$. (a) Top and side views of crystal structure of monolayer $NaW_2O_2Br_6$. Blue, brown, red and purple balls represent W, Br, O, and Na atoms, respectively. W atoms are coordinated by two O atoms and four Br atoms to form WO_2Br_4 octahedra. (b) Real space electron density distribution of monolayer $NaW_2O_2Br_6$. (c) The line plot electron density distribution of the red dashed line in (b). (d) Such electron distribution can be regarded as a natural metal/dielectric multilayer, a typical hyperbolic metamaterial system.

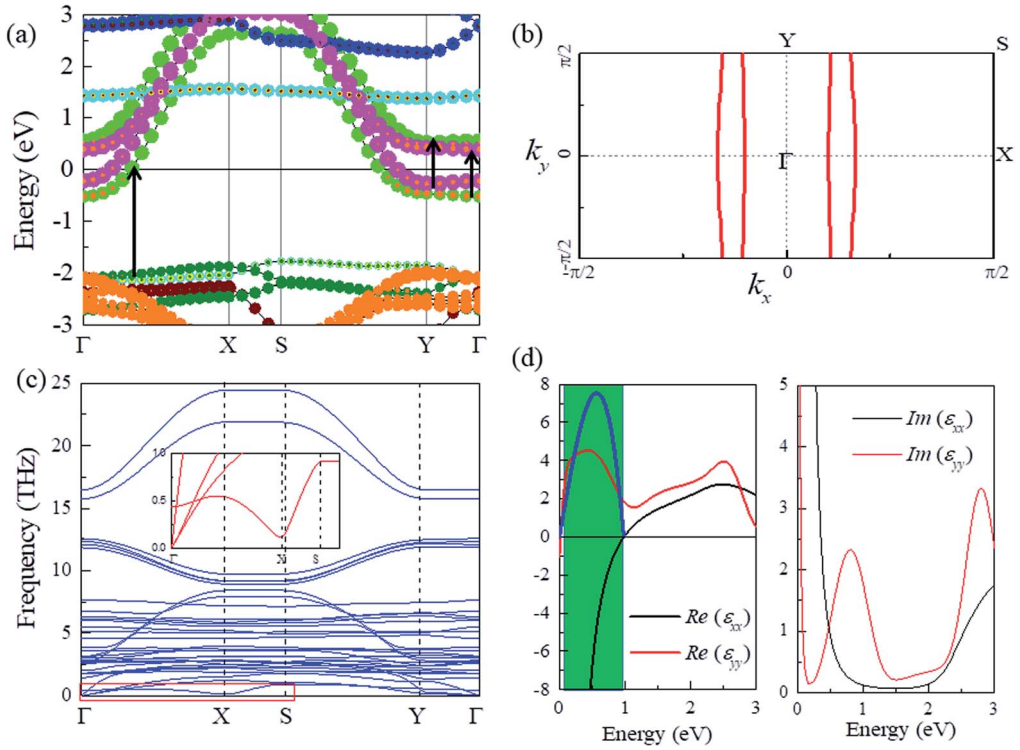

Fig. 2 Extremely anisotropic electronic properties and hyperbolic PPs. (a) Orbital projected band structure for monolayer $NaW_2O_2Br_6$. Green, blue, cyan, and purple dots represent d_{xy}, d_{yz}, d_z^2 and d_{xz} orbitals of W atoms, respectively. Orange, wine and olive dots (b) represent p_x, p_y and p_z orbitals of Br atoms, respectively. (c) The phonon dispersion of monolayer $NaW_2O_2Br_6$. The inset (red line) is the magnification of phonon dispersion around the *X* point. (d) The real and imaginary parts of dielectric functions along *x* and *y* directions, respectively. Between 0.03 and 0.98 eV, it is hyperbolic for Re(ε_{yy}) is positive, whereas Re(ε_{xx}) is negative. The blue line in (d) is the FoM in the hyperbolic range.

different directions. For monolayer $NaW_2O_2Br_6$, it is quite different. As shown in Fig. 2a, for the *x* direction (*Γ* to *X* and *Y* to *S* paths), two well dispersed bands, contributed by d_{xz} and d_{xy} orbitals, respectively, cross the Fermi level. But for the *y* direction (*Γ* to *Y* and *X* to *S* paths), no band crosses the Fermi level, and it looks like a semiconductor with rather flat conduction and valence bands. Both the highest occupied band and the lowest unoccupied band are mainly composed of the d_{xz} orbital. These extremely anisotropic electronic properties are consistent with our previous analysis by the charge density that monolayer $NaW_2O_2Br_6$ is like a 2D metal/dielectric multilayer.

To further demonstrate this extremely anisotropic metallic property, we plot the Fermi surface (FS) for monolayer $NaW_2O_2Br_6$ in Fig. 2b. Notably, it displays an extremely anisotropic character: there are two sets of almost parallel lines along the k_y direction. As a result, no band crosses the Fermi level along the *y* direction. Materials with such extremely anisotropic FSs usually are unstable at low temperature, which may induce metal-insulator transitions due to Peierls transition.[29,30] But for practical photonic applications, it is important to have the devices work at room temperature. At room temperature, it would be an anisotropic metal as we calculated. Phonon dispersion shows no imaginary frequency, indicating that this extremely anisotropic metallic state could be dynamically stable (Fig. 2c). Meanwhile, we also calculated the cleavage energy by separating a $NaW_2O_2Br_6$ monolayer from neighboring five layers. The corresponding cleavage energy is 0.26 J m^{-2} (supplied in the ESI, Fig. S1†), which is quite small, indicating that the exfoliation of the $NaW_2O_2Br_6$ monolayer from its bulk phase is expected to be highly feasible. So, here we directly consider this anisotropic metallic state for monolayer $NaW_2O_2Br_6$, even there might be phase changes at low temperature.

Monolayer $NaW_2O_2Br_6$: a hyperbolic plasmonic surface

Usually, anisotropic metallic properties could result in anisotropic plasmonic properties. The optical properties of metals are usually dominated by intraband transitions in low energy regions, which can be expressed by the Drude model:[31]

$$\varepsilon^{\text{intra}} = \varepsilon_\infty - \frac{\omega_p^2}{\omega^2 + i\gamma\omega} \quad (1)$$

where ε_∞ is the static dielectric constant, and γ is the damping coefficient. As we see, anisotropic plasma frequencies could result in hyperbolic properties, for Re(ε_{xx}) and Re(ε_{yy}), the real part of dielectric functions, could have opposite signs in some regions. The plasma frequency tensors can be directly calculated from the electronic band structures by[32]

$$\omega_{p\alpha\alpha}^2 = -\frac{8\pi e^2}{V}\sum_{n,\boldsymbol{k}} v_{nk_\alpha}^2 \frac{\partial f_{n\boldsymbol{k}}}{\partial \epsilon_{n\boldsymbol{k}}} \quad (2)$$

where V is the cell volume, $v_{nk_\alpha} = \frac{\partial \epsilon_{nk}}{\hbar\, \partial k_\alpha}$ is the group velocity, and f_{nk} is the quasiparticle distribution function. As we see, the plasma frequency is contributed by v_{nk_α} for every k point at the FS. According to the FS in Fig. 2b, it is almost independent of k_y, indicating a nearly zero ω_{pyy}, but a finite ω_{pxx}. So, monolayer $NaW_2O_2Br_6$ could be a natural candidate to host hyperbolic PPs. Confirmed by our DFT calculations, the ω_{pxx} and ω_{pyy} are calculated to be 1.52 and 0.12 eV, respectively. We also considered the contributions from interband transitions for monolayer $NaW_2O_2Br_6$ (Fig. S2†). In Fig. 2d, a hyperbolic window, from 0.03 to 0.98 eV, is observed ($\gamma \sim 50$ meV), in which $\mathrm{Re}(\varepsilon_{yy})$ is positive, whereas $\mathrm{Re}(\varepsilon_{xx})$ is negative. The influence of γ on hyperbolic properties is also evaluated by other values ($\gamma = 0.1$ and 0.02 eV) (Fig. S3†). The results show that they have a negative influence on the hyperbolic properties, especially the hyperbolic window. The hyperbolic window is very broad, ranging from far-infrared (FIR) (40 μm) to NIR light (1.3 μm). Such a broad hyperbolic window is mainly due to the large difference between ω_{pxx} and ω_{pyy}. We notice that such a broad hyperbolic window is never reported in traditional artificial metal/dielectric multilayers. Meanwhile, no interband transition occurs in the hyperbolic region for the x direction, indicating the negligible optical losses. To directly compare and quantify the losses of various hyperbolic surfaces, the figure of merit (FoM) is commonly used, defined as[28]

$$\mathrm{FoM} = -\frac{\mathrm{Re}(\varepsilon)}{\mathrm{Im}(\varepsilon)} \quad (3)$$

where $\mathrm{Re}(\varepsilon)$ and $\mathrm{Im}(\varepsilon)$ are the real and imaginary parts of dielectric functions for the $\mathrm{Re}(\varepsilon) < 0$ direction, respectively. As observed in Fig. 2d (blue line), the maximum FoM can be up to 7.3 around 0.56 eV, and it can be over 1 within a wide range, from FIR (30 μm) to NIR (1.3 μm). The reported as hyperbolic PhPs, BN and MoO_3, could exhibit much higher FoMs, up to 200.[4–6] However, their hyperbolic windows are very narrow, and the high FoM is only located in a very small region in the range of mid-infrared (MIR). Thus, a broad hyperbolic window, ranging from FIR to NIR, and a considerable FoM make monolayer $NaW_2O_2Br_6$ have great potential for application in hyperbolic optical devices.

Carrier tunable hyperbolic properties in monolayer $NaW_2O_2Br_6$

Based on the electronic structure (Fig. 2a), monolayer $NaW_2O_2Br_6$ is an anisotropic metal. Usually, the properties of metals, including the plasmonic properties, do not respond to the carrier doping, due to their high intrinsic carrier concentrations.[33] $MoOCl_2$ (ref. 24) and CuB_3 (ref. 25) could display hyperbolic properties even in the UV range, due to their larger plasmonic frequencies. However, to tune their hyperbolic properties, the carrier density should be up to 10^{14} cm^{-2}, which is hard to realize in experiment. Luckily, the intrinsic carrier concentration in monolayer $NaW_2O_2Br_6$ is only about 2.5×10^{14} cm^{-2}, about one order less than that in these 2D metals, which even can be recognized as an anisotropic semiconductor with an electron doping concentration of 2.5×10^{14} cm^{-2}. Attributed to such low intrinsic electron concentration, the plasmonic properties in monolayer $NaW_2O_2Br_6$ could be modified by carriers with the density at the order of 10^{13} cm^{-2}. Such required carrier density is about one order less than those for 2D metals and semiconductors, which shows great potential in real applications. To reveal this, we investigate these hyperbolic PPs in monolayer $NaW_2O_2Br_6$ upon carrier doping.

The carrier doped electronic structures of monolayer $NaW_2O_2Br_6$ are displayed in Fig. 3a. The doping carrier density ranges from -2.5×10^{13} cm^{-2} (hole) to 8.75×10^{13} cm^{-2} (electron). As we see, among this doping range, the Fermi level is gradually shifted without changing the shape of FSs (Fig. 3b). Electron doping will move the Fermi level upwards, and it is opposite for hole doping. We also found that the plasma frequency, ω_{pxx}, shows a good dependence on carrier concentration with the relation of $\omega_p^2 = ne^2/\varepsilon_0 m^*$ (Fig. 3c). The bands crossing the Fermi level exhibit well-defined dispersions on k_x^2, suggesting that the carrier mass is independent of carrier concentration. In this doping range, the FSs show a similar dependence on k_y, indicating almost unchanged ω_{pyy}. Thus, we can expect a predictable tunable hyperbolic behavior: carrier doping can gradually shift the upper limit of the hyperbolic region: electrons blueshift it, and holes redshift it, while the lower limit is almost independent of the carrier. As confirmed by the dielectric functions in Fig. 4a and b, the hyperbolic window can be changed from (0.03, 0.98) eV without doping to (0, 1.27) eV for electron doping of 8.75×10^{13} cm^{-2}, and also to (0.05, 0.88) eV for hole doping of 2.5×10^{13} cm^{-2}. It means that in the range of (0.88, 1.27) eV, whether hyperbolic or elliptic, it depends on carrier concentration.

For hyperbolic optical devices, except the hyperbolic windows, other properties are also very important for applications, such as FoM and the propagation direction of the plasmon beams. The FoM upon the carrier density of monolayer $NaW_2O_2Br_6$ is plotted in Fig. 4c. The color region is hyperbolic, while the other region is elliptic. We found that the highest FoM can be enhanced and gradually blueshifted with the electron doping. The best FoM is about 7.3 at 0.56 eV without doping, and it increases to about 9.9 at 0.75 eV with an electron doping concentration of 8.75×10^{13} cm^{-2}. Interestingly, although it is hyperbolic from FIR to NIR, the tunability upon carrier density is different. As shown in Fig. 4c, below about 0.4 eV, the FoM is not sensitive to carrier concentration. In the range between 0.4 and 0.88 eV, increasing the electron density would significantly improve the FoM. Above 0.88 eV, the topological transition between elliptic and hyperbolic can occur, and the FoM can also be dramatically enhanced. As we see, it is elliptic at 0.9 eV with a hole doping concentration of 2.5×10^{13} cm^{-2}. It changes to hyperbolic with the FoM quickly increasing to 9.0 at an electron doping concentration of 8.75×10^{13} cm^{-2}. Thus, although the hyperbolic window can cover almost the whole IR light, only NIR light can be tuned by carrier density, not FIR and MIR light.

Similar tunable behavior is also found for the direction of the plasmon beams. In the hyperbolic range, the plasmon beams are significantly more localized than the elliptic case,

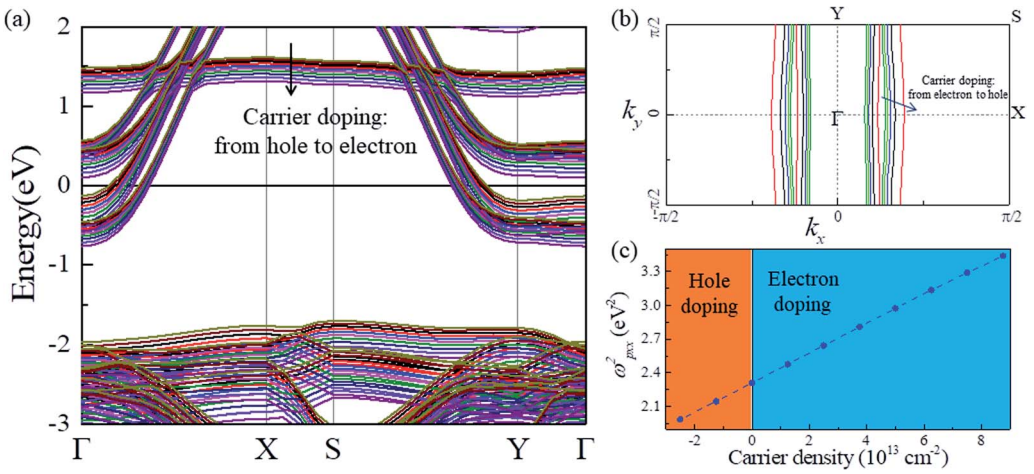

Fig. 3 Carrier tunable electronic properties of monolayer $NaW_2O_2Br_6$. (a) Band structures under carrier doping from -2.5×10^{13} cm^{-2} (hole) to 8.75×10^{13} cm^{-2} (electron). (b) The Fermi surfaces with the carrier doping concentration of -2.5 (red), 0 (black), 2.5 (blue), 5.0 (green), and 7.5 (olive) $\times 10^{13}$ cm^{-2}, respectively. (c) The dependence of ω_p^2 on carrier doping concentration.

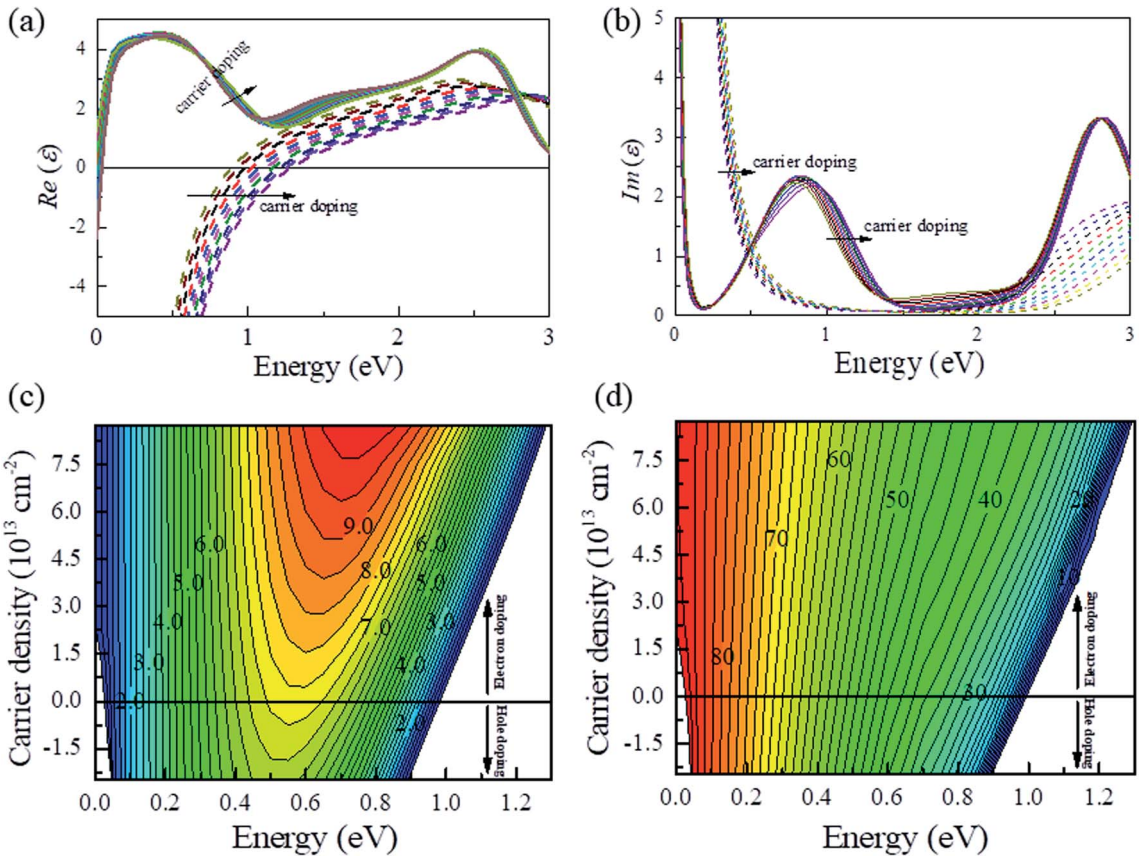

Fig. 4 Tunable hyperbolic properties of monolayer $NaW_2O_2Br_6$ upon carrier density. (a and b) The real and imaginary parts of dielectric functions of monolayer $NaW_2O_2Br_6$ upon carrier doping, respectively. The arrows indicate the carrier doping from holes to electrons. (c and d) The counter mapping of FoM and propagation direction (respect to the y axis) of the plasmon beams upon carrier doping, respectively.

because plasmons with all momenta carry energy along the direction of the hyperbola asymptotes defined by[18]

$$y = \pm x\sqrt{\left|\mathrm{Re}(\varepsilon_{yy})/\mathrm{Re}(\varepsilon_{xx})\right|} \quad (4)$$

Usually, the direction of the plasmon beams is also defined by the direction of asymptotes. Fig. 4d displays the propagation directions of plasmon beams by the angle between the y axis and plasmon beams. As we see, the propagation directions of

MIR and FIR lights are mainly restrained along the x direction, and they show little dependence on carrier density. For NIR light above 0.4 eV, its propagation directions can be controlled by carrier density. For example, the angle can be rotated from 40° to 54° for the light of 0.6 eV, when the doped carrier concentration changes from holes of 2.5×10^{13} cm^{-2} to electrons of 8.75×10^{13} cm^{-2}. Above 0.9 eV, the propagation directions of plasmon beams can also be tuned when the topology transition between elliptic and hyperbolic occurs. This indicates that carrier concentration not only can control the hyperbolic window and their FoMs, but also can control the propagation behaviors.

These tunable hyperbolic properties are due to the extremely anisotropic electronic properties in monolayer $NaW_2O_2Br_6$. Interestingly, we also found that the tunable behavior upon carrier concentration is also extremely anisotropic. By the dielectric properties, including Im(ε) and Re(ε), shown in Fig. 4a and b, the absorption peaks around 0.9 eV and 2.7 eV for the y direction are nearly independent of the carrier concentration. The absorption peak around 0.9 eV is due to the interband transitions from the d_{xz} (d_{xy}) orbital below the Fermi level to the d_{xy} (d_{xz}) orbital above the Fermi level, as illustrated in Fig. 2a. Shifting the Fermi level by carrier concentration has a negligible effect on this transition. It is similar for the absorption peaks around 2.7 eV. But in the x direction, the optical transitions from the d_{xz} (d_{xy}) orbital below the Fermi level to the d_{xy} (d_{xz}) orbital are optically forbidden. The absorption starting from 2.0 eV for the x direction is due to the interband transition from bands around −2 eV to the bands above the Fermi level. This interband transition is carrier dependent in a mechanism like the Burstein–Moss effect. Such extremely anisotropic properties, especially the anisotropic tunable behavior, are never reported in other materials, endowing monolayer $NaW_2O_2Br_6$ with particular potential in electrically controlling directional optical devices.

Tunable hyperbolic PPs by solid-gated FETs

From the perspective of potential applications, the ability to integrate hyperbolic PhPs into nanophotonic and optoelectronic circuits is highly desirable. Based on the first-principles calculations, a carrier density at the order of 10^{13} cm^{-2} can effectively modulate the hyperbolic performance in monolayer $NaW_2O_2Br_6$, including the hyperbolic window, FoM and the propagation direction of plasmon beams. Such carrier density usually can be easily realized in electric double layer transistors (EDLTs)[34,35] by using polymer electrolytes or ionic liquids as gated dielectrics. But EDLTs are not feasible for integrating these hyperbolic properties into nano-optoelectronic devices. Luckily, it is reported that such carrier density could also be approached in some well-fabricated solid-gated FETs,[36,37] which makes a possibility for the design of gate tunable hyperbolic photonic devices. Thus, we propose a gate tunable hyperbolic device based on solid-gated FETs with monolayer $NaW_2O_2Br_6$ as the channel. The schematic device is shown in Fig. 5, where the bottom gate supplies the electric field to control the propagation behaviors of NIR light in monolayer $NaW_2O_2Br_6$. According to the calculations, when a NIR light propagates in monolayer $NaW_2O_2Br_6$, the propagation direction, the FoM, and even the topology (elliptic and hyperbolic) of NIR light can be controlled by the gate voltage, depending on the light wavelength. The ability to integrate with FETs enables electrical control of optical signals in monolayer $NaW_2O_2Br_6$, which has significant implications on integrating photonics and nano-optoelectronics into a single chip and also other novel optoelectronic devices. For example, hyperbolic PPs can support the plasmonic spin-Hall effect.[38] In the range of (0.88, 1.27) eV, it is hyperbolic or elliptic depending on the carrier density, *i.e.*, the gate voltage. It means that the plasmonic spin-Hall effect for NIR light can be switched by the gate voltage in monolayer $NaW_2O_2Br_6$.

As we discussed above, the hyperbolic PPs in monolayer $NaW_2O_2Br_6$ are mainly due to the extremely anisotropic

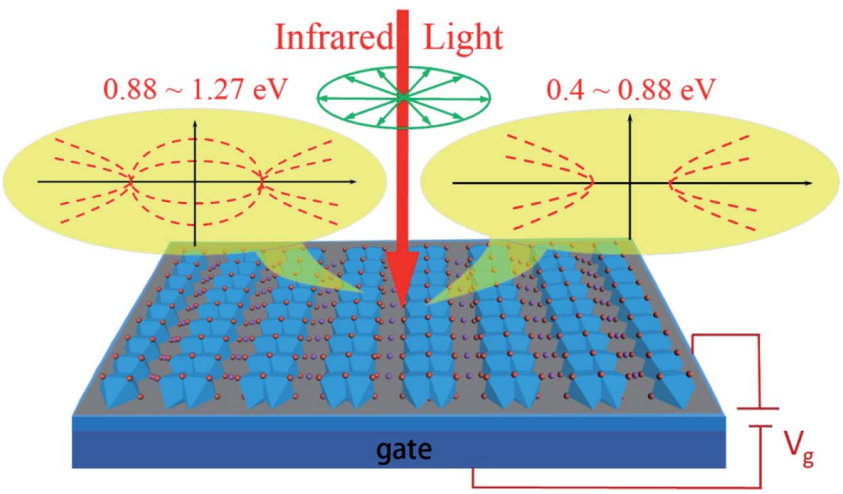

Fig. 5 Schematic diagram of the gate tunable NIR hyperbolic device by FETs. When a NIR incident light illuminated on monolayer $NaW_2O_2Br_6$, the propagation behaviors of NIR light in monolayer $NaW_2O_2Br_6$, including the propagation direction, the FoM, and even the topology (depending on the wavelength of NIR light), can be manipulated by the gate voltage.

electronic properties. Except the electronic properties, the tunability in optical properties upon carrier density is also extremely anisotropic, indicating that other properties in monolayer $NaW_2O_2Br_6$, such as mechanic, transport, and thermal properties, could also be extremely anisotropic. For example, the thermal conductivity as known is contributed by both phonons and electrons. In monolayer $NaW_2O_2Br_6$, it is conducting for the *y* direction but almost insulating for the *x* direction, suggesting the extremely anisotropic thermal conductivity from electron contribution. Such extremely anisotropic properties in monolayer $NaW_2O_2Br_6$ would also open opportunities for novel functional anisotropic devices.

In conclusion, we propose that monolayer $NaW_2O_2Br_6$ is a natural candidate for infrared hyperbolic PPs with extraordinary properties, such as broad hyperbolic window and considerable FoM, because of its extremely anisotropic structural and metallic properties. Owing to the low intrinsic carrier concentration, hyperbolic PPs in monolayer $NaW_2O_2Br_6$ for NIR light can be manipulated by the gate voltage in solid-gated FETs, which provides great potential for application in integrating tunable polaritons into nano-optoelectronic devices. We anticipate our work will promote more experimental and theoretical efforts on the realization of integrable hyperbolic PPs based on 2D materials.

Methods

Electronic calculation for monolayer $NaW_2O_2Br_6$

The electronic and dielectric properties of monolayer $NaW_2O_2Br_6$ are calculated by the Vienna *ab initio* Simulation Package (VASP)[39,40] based on density functional theory (DFT). The electronic structures are described by using the generalized gradient approximation (GGA) based Perdew–Burke–Ernzerhof (GGA-PBE) exchange–correlation functional[41] with the projector augmented wave (PAW).[42] The cutoff energy used for the plane-wave basis set is 450 eV for monolayer $NaW_2O_2Br_6$. The structures are relaxed until the atomic forces are less than 0.01 eV per Å per atom and total energies are converged to 10^{-5} eV. Vacuum layers of 15 Å are inserted between the periodically repeated slabs along the *c*-axis to avoid interactions among them caused by the periodic boundary conditions for both. The PBE exchange–correlation functional usually underestimates both band gaps of semiconductors and interband transition energies in metals. We applied a hybrid functional (HSE06)[43] to compute the electronic structures of monolayer $NaW_2O_2Br_6$, which generally yields more reliable band energies. Finer *k*-point samplings of 80 × 30 × 1 are used to calculate FSs.

Dielectric calculation for monolayer $NaW_2O_2Br_6$

We apply the independent particle approximation to describe the dielectric function from electronic band structure calculations. The dielectric function $\varepsilon(\omega) = \varepsilon_1(\omega) + i\varepsilon_2(\omega)$ (where ε_1 is the real part, and ε_2 is the imaginary part) of metals in the low-frequency region is contributed by two important processes, interband ($\varepsilon^{\text{inter}}(\omega)$) and intraband ($\varepsilon^{\text{intra}}(\omega)$) transitions.

The imaginary part of the dielectric function contributed by interband transition is calculated by[44]

$$\varepsilon_2^{\text{inter}}(\omega) = \frac{4\pi^2 e^2}{\Omega} \lim_{q\to 0} \frac{1}{q^2} \sum_{c,v,\boldsymbol{k}} 2w_{\boldsymbol{k}} \delta(E_{c\boldsymbol{k}} - E_{v\boldsymbol{k}} - \omega) \times \left| \left\langle u_{c\boldsymbol{k}+q} | u_{v\boldsymbol{k}} \right\rangle \right|^2 \tag{5}$$

where *e* is the electron charge, Ω is the primitive cell volume, and $w_{\boldsymbol{k}}$ is the weight of the $\boldsymbol{k}$-points. The indices *c* and *v* refer to the CB and VB states, respectively. The parameter $E_{j\boldsymbol{k}}$ is the single-electron energy state of band *j* at wave vector $\boldsymbol{k}$, $u_{j\boldsymbol{k}}$ is the periodic part of the Bloch wave function corresponding to the eigenvalue $E_{i\boldsymbol{k}}$ ($i = c, v$), and δ is the delta function, which depends upon the method used for calculation. The real part of the dielectric function contributed by interband transition is obtained from the Kramers–Kronig relation.

The dielectric function for intraband transitions, $\varepsilon^{\text{intra}}(\omega)$, is known as the dielectric function of a free electron gas. The contribution by intraband transitions, $\varepsilon^{\text{intra}}(\omega)$, is obtained by Drude expression for a given plasma frequency ω_p and damping constant (γ):[31]

$$\varepsilon^{\text{intra}} = \varepsilon_\infty - \frac{{\omega_p}^2}{\omega^2 + i\gamma\omega} \tag{6}$$

while ω_p can be calculated from the electronic band structure as follows:[32]

$${\omega_{p\alpha\alpha}}^2 = -\frac{8\pi e^2}{V} \sum_{n,\boldsymbol{k}} {v_{nk_\alpha}}^2 \frac{\partial f_{n\boldsymbol{k}}}{\partial \epsilon_{n\boldsymbol{k}}} \tag{7}$$

Dense *k*-point samplings of 100 × 40 × 1 are applied to calculate the dielectric properties of monolayer $NaW_2O_2Br_6$. The total dielectric function is the sum of the dielectric functions for inter- and intraband transitions: $\varepsilon(\omega) = \varepsilon^{\text{inter}}(\omega) + \varepsilon^{\text{intra}}(\omega)$.

Conflicts of interest

The authors declare no competing interests.

Acknowledgements

B. X. acknowledges the support from "Double First-Class" University project of China Pharmaceutical University (CPU2018GFY25).

References

1 D. N. Basov, M. M. Fogler and F. J. G. de Abajo, Polaritons in van der Waals materials, *Science*, 2016, **354**, 1992.
2 T. Low, A. Chaves, J. D. Caldwell, A. Kumar, N. X. Fang, P. Avouris, T. F. Heinz, F. Guinea, L. Martin-Moreno and F. Koppens, Polaritons in layered two-dimensional materials, *Nat. Mater.*, 2017, **16**, 182–194.
3 Q. Zhang, G. W. Hu, W. L. Ma, P. N. Li, A. Krasnok, R. Hillenbrand, A. Alu and C. W. Qiu, Interface nano-optics with van der Waals polaritons, *Nature*, 2021, **597**, 187–195.

4 A. Woessner, M. B. Lundeberg, Y. Gao, A. Principi, P. Alonso-Gonzaolez, M. Carrega, K. Watanabe, T. Taniguchi, G. Vignale, M. Polini, J. Hone, R. Hillenbrand and F. H. L. Koppens, Highly confined low-loss plasmons in graphene-boron nitride heterostructures, *Nat. Mater.*, 2015, **14**, 421–425.

5 P. N. Li, I. Dolado, F. J. Alfaro-Mozaz, F. Casanova, L. E. Hueso, S. Liu, J. H. Edgar, A. Y. Nikitin, S. Velez and R. Hillenbrand, Infrared hyperbolic metasurface based on nanostructured van der Waals materials, *Science*, 2018, **359**, 892–896.

6 S. Dai, Z. Fei, Q. Ma, A. S. Rodin, M. Wagner, A. S. McLeod, M. K. Liu, W. Gannett, W. Regan, K. Watanabe, T. Taniguchi, M. Thiemens, G. Dominguez, A. H. Castro Neto, A. Zettl, F. Keilmann, P. Jarillo-Herrero, M. M. Fogler and D. N. Basov, Tunable Phonon Polaritons in Atomically Thin van der Waals Crystals of Boron Nitride, *Science*, 2014, **343**, 1125–1129.

7 W. L. Ma, P. Alonso-Gonzalez, S. J. Li, A. Y. Nikitin, J. Yuan, J. Martin-Sanchez, J. Taboada-Gutierrez, I. Amenabar, P. N. Li, S. Velez, C. Tollan, Z. G. Dai, Y. P. Zhang, S. Sriram, K. Kalantar-Zadeh, S. T. Lee, R. Hillenbrand and Q. L. Bao, In-plane anisotropic and ultra-low-loss polaritons in a natural van der Waals crystal, *Nature*, 2018, **562**, 557–562.

8 G. W. Hu, Q. D. Ou, G. Y. Si, Y. J. Wu, J. Wu, Z. G. Dai, A. Krasnok, Y. Mazor, Q. Zhang, Q. L. Bao, C. W. Qiu and A. Alu, Topological polaritons and photonic magic angles in twisted alpha-MoO_3 bilayers, *Nature*, 2020, **582**, 209–213.

9 Z. B. Zheng, N. S. Xu, S. L. Oscurato, M. Tamagnone, F. S. Sun, Y. Z. Jiang, Y. L. Ke, J. N. Chen, W. C. Huang, W. L. Wilson, A. Ambrosio, S. Z. Deng and H. J. Chen, A mid-infrared biaxial hyperbolic van der Waals crystal, *Sci. Adv.*, 2019, **5**, eaav8690.

10 Q. Zhang, Q. D. Ou, G. W. Hu, J. Y. Liu, Z. G. Dai, M. S. Fuhrer, Q. L. Bao and C. W. Qiu, Hybridized hyperbolic surface phonon polaritons at alpha-MoO_3 and polar dielectric interfaces, *Nano Lett.*, 2021, **21**, 3112–3119.

11 J. Taboada-Gutierrez, G. Alvarez-Perez, J. H. Duan, W. L. Ma, K. Crowley, I. Prieto, A. Bylinkin, M. Autore, H. Volkova, K. Kimura, T. Kimura, M. H. Berger, S. J. Li, Q. L. Bao, X. P. A. Gao, I. Errea, A. Y. Nikitin, R. Hillenbrand, J. Martin-Sanchez and P. Alonso-Gonzalez, Broad spectral tuning of ultra-low-loss polaritons in a van der Waals crystal by intercalation, *Nat. Mater.*, 2020, **19**, 964–968.

12 A. N. Grigorenko, M. Polini and K. S. Novoselov, Graphene plasmonics, *Nat. Photonics*, 2012, **6**, 749–758.

13 Z. Fei, A. S. Rodin, G. O. Andreev, W. Bao, A. S. McLeod, M. Wagner, L. M. Zhang, Z. Zhao, M. Thiemens, G. Dominguez, M. M. Fogler, A. H. Castro Neto, C. N. Lau, F. Keilmann and D. N. Basov, Gate-tuning of graphene plasmons revealed by infrared nano-imaging, *Nature*, 2012, **487**, 82–85.

14 G. X. Ni, A. S. McLeod, Z. Sun, L. Wang, L. Xiong, K. W. Post, S. S. Sunku, B. Y. Jiang, J. Hone, C. R. Dean, M. M. Fogler and D. N. Basov, Fundamental limits to graphene plasmonics, *Nature*, 2018, **557**, 530–533.

15 J. S. Gomez-Diaz and A. Alu, Flatland optics with hyperbolic metasurfaces, *ACS Photonics*, 2016, **3**, 2211–2224.

16 J. S. Gomez-Diaz, M. Tymchenko and A. Alu, Hyperbolic plasmons and topological transitions over uniaxial metasurfaces, *Phys. Rev. Lett.*, 2015, **114**, 233901.

17 C. Wang, S. Y. Huang, Q. X. Xing, Y. G. Xie, C. Y. Song, F. J. Wang and H. G. Yan, Van der Waals thin films of WTe_2 for natural hyperbolic plasmonic surfaces, *Nat. Commun.*, 2020, **11**, 1158.

18 Z. Torbatian, D. Novko and R. Asgari, Tunable Low-Loss Hyperbolic Plasmon Polaritons in a T_d-WTe_2 Single Layer, *Phys. Rev. Appl.*, 2020, **14**, 044014.

19 A. Nemilentsau, T. Low and G. Hanson, Anisotropic 2D materials for tunable hyperbolic plasmonics, *Phys. Rev. Lett.*, 2016, **116**, 066804.

20 E. Veen, A. Nemilentsau, A. Kumar, R. Roldan, M. I. Katsnelson, T. Low and S. J. Yuan, Tuning two-dimensional hyperbolic plasmons in black phosphorus, *Phys. Rev. Appl.*, 2019, **12**, 014011.

21 J. A. Silva-Guillen, E. Canadell, F. Guinea and R. Roldan, Strain tuning of the anisotropy in the optoelectronic properties of TiS_3, *ACS Photonics*, 2018, **5**, 3231–3237.

22 Y. F. Huang, S. N. Shirodkar and B. I. Yakobson, Two-dimensional boron polymorphs for visible range plasmonics: A first-principles exploration, *J. Am. Chem. Soc.*, 2017, **139**, 17181–17185.

23 C. Lian, S. Q. Hu, J. Zhang, C. Cheng, Z. Yuan, S. W. Gao and S. Meng, Integrated plasmonics: broadband dirac plasmons in borophene, *Phys. Rev. Lett.*, 2020, **125**, 116802.

24 J. Z. Zhao, W. K. Wu, J. J. Zhu, Y. H. Lu, B. Xiang and S. Y. A. Yang, Highly anisotropic two-dimensional metal in monolayer $MoOCl_2$, *Phys. Rev. B: Condens. Matter Mater. Phys.*, 2020, **102**, 245419.

25 W. H. Geng, H. Gao, C. Ding, L. Sun, X. K. Ma, Y. Y. Li and M. W. Zhao, Highly-anisotropic plasmons in two-dimensional hyperbolic copper borides, *Opt. Express*, 2022, **30**, 5596–5607.

26 Y. Q. Zheng, K. Peters and H. G. von Schnering, The mixed valence tungsten(IV,V) compound $Na[W_2O_2Br_6]$, *Z. Anorg. Allg. Chem.*, 1998, **624**, 1415–1418.

27 K. Andersen and K. S. Thygesen, Plasmons in metallic monolayer and bilayer transition metal dichalcogenides, *Phys. Rev. B: Condens. Matter Mater. Phys.*, 2013, **88**, 155128.

28 A. Poddubny, I. Iorsh, P. Belov and Y. Kivshar, Hyperbolic metamaterials, *Nat. Photonics*, 2013, **7**, 948–957.

29 D. Hirai, M. Bremholm, J. M. Allred, J. Krizan, L. M. Schoop, Q. Huang, J. Tao and R. J. Cava, Spontaneous formation of zigzag chains at the metal-insulator transition in the beta-pyrochlore CsW_2O_6, *Phys. Rev. Lett.*, 2013, **110**, 166402.

30 K. N. Zhang, X. Y. Liu, H. X. Zhang, K. Deng, M. Z. Yan, W. Yao, M. T. Zheng, E. F. Schwier, K. Shimada, J. D. Denlinger, Y. Wu, W. H. Duan and S. Y. Zhou, Evidence for a quasi-one-dimensional charge density wave in cuTe by angle-resolved photoemission spectroscopy, *Phys. Rev. Lett.*, 2018, **121**, 206402.

31 S. A. Maier, *Plasmonics, Fundamentals and Applications*, Springer, 2007, vol. 26, p. 224.

32 K. H. Lee and K. J. Chang, First-principles study of the optical properties and the dielectric response of Al, *Phys. Rev. B: Condens. Matter Mater. Phys.*, 1994, **49**, 2362–2367.
33 R. A. Maniyara, D. Rodrigo, R. Yu, J. Canet-Ferrer, D. S. R. Ghosh, R. Yongsunthon, D. E. Baker, A. Rezikyan, F. J. G. de Abajo and V. Pruneri, Tunable plasmons in ultrathin metal films, *Nat. Photonics*, 2019, **13**, 328–333.
34 D. Braga, I. G. Lezama, H. Berger and A. F. Morpurgo, Quantitative determination of the band gap of WS_2 with ambipolar ionic liquid-gated transistors, *Nano Lett.*, 2012, **12**, 5218–5223.
35 D. K. Efetov and P. Kim, Controlling electron-phonon interactions in graphene at ultrahigh carrier densities, *Phys. Rev. Lett.*, 2010, **105**, 256805.
36 Y. J. Zhang, J. T. Ye, Y. Matsuhashi and Y. Iwasa, Ambipolar MoS_2 Thin Flake Transistors, *Nano Lett.*, 2012, **12**, 1136–1140.
37 K. F. Mak, K. L. He, C. Lee, G. H. Lee, J. Hone, T. F. Heinz and J. Shan, Ambipolar MoS_2 thin flake transistors, *Nat. Mater.*, 2013, **12**, 207–211.
38 A. A. High, R. C. Devlin, A. Dibos, M. Polking, D. S. Wild, J. Perczel, N. P. de Leon, M. D. Lukin and H. Park, Visible-frequency hyperbolic metasurface, *Nature*, 2015, **522**, 192–196.
39 G. Kresse and J. Hafner, Ab initio molecular dynamics for open-shell transition metals, *Phys. Rev. B: Condens. Matter Mater. Phys.*, 1993, **48**, 13115.
40 G. Kresse and J. Furthmuller, Efficient iterative schemes for *ab initio* total-energy calculations using a plane-wave basis set, *Phys. Rev. B: Condens. Matter Mater. Phys.*, 1996, **54**, 11169.
41 J. P. Perdew, K. Burke and M. Ernzerhof, Generalized gradient approximation made simple, *Phys. Rev. Lett.*, 1996, **77**, 3865.
42 P. E. Blochl, Projector augmented-wave method, *Phys. Rev. B: Condens. Matter Mater. Phys.*, 1994, **50**, 17953.
43 J. Heyd, G. E. Scuseria and M. Ernzerhof, Hybrid functionals based on a screened Coulomb potential, *J. Chem. Phys.*, 2003, **118**, 8207–8215.
44 M. Gajdos, K. Hummer, G. Kresse, J. Furthmuller and F. Bechstedt, Linear optical properties in the projector-augmented wave methodology, *Phys. Rev. B: Condens. Matter Mater. Phys.*, 2006, **73**, 045112.